Magnetic and Transport Properties of Some Mixed-Valent Niobium Phosphates

A. Benabbas, J. Provost, M. M. Borel,* A. Leclaire, and B. Raveau

Laboratoire Crismat, ISMRA/Université de Caen, Boulevard du Maréchal Juin, 14050 Caen Cedex, France

Received April 7, 1993. Revised Manuscript Received June 3, 1993

Polycrystalline samples and single crystals of some mixed-valent niobium phosphates have been synthesized. Their magnetic and transport properties have been studied in the 4.5–300 K temperature range. All the samples exhibit semiconducting behavior. The electrical resistivity along the crystallographic axis of the single crystals have been related to the structure of the chains of NbO_6 octahedra and mainly to the angle between Nb–O–Nb bonds. The magnetic susceptibility data have been related to the location of Nb^V and of Nb^{IV} in the octahedra of ReO_3-type layers based on octahedral distortion considerations and on the distance between Nb ions, which does not allow magnetic ordering when the distance is too large. In the case of potassium phosphate bronzes some deviations from the theoretical values of μ_B are interpreted in term of potassium nonstoichiometry.

Introduction

After the discovery of tungsten phosphate bronzes (for a review see refs 1 and 2), a great deal of work was devoted to the electron-transport properties of these materials owing to their low dimensionality. Very interesting properties, such as resistivity anomalies related to a charge density wave (CDW), have been observed, that were interpreted on the basis of band electronic structure calculations.[3-11] In these structures the conducting properties are closely related to the geometry of the chains of WO_6 octahedra that form the ReO_3-type layers.

Niobium, owing to its ability to exhibit the mixed valence Nb^V–Nb^{IV} and to form niobium phosphates built up from octahedral chains, is well suited to exhibit similar properties. Recently new structural families of niobium phosphate bronzes were isolated. In the system K–Nb–P–O, three series of phosphates were synthesized: $KNb_3P_3O_{15}$[12] related to the tetragonal bronze (TTB), $K_3Nb_6P_4O_{26}$[13] derived from the hexagonal tungsten bronze (HTB), $K_7Nb_{14}P_9O_{60}$,[14] α-$K_{5-x}Nb_8P_5O_{34}$,[15] and β-$K_2Na_{2-x}Nb_8P_5O_{34}$[16] related to the intergrowth tungsten bronzes (ITB). In the system Na–Nb–P–O, the bronzes $Na_4Nb_8P_4O_{32}$,[17] $Na_{4-x}Nb_7P_4O_{29}$,[18] and $Na_{2+x}Nb_6P_4O_{26}$[19] that exhibit the structure of monophosphate tungsten bronze with pentagonal tunnels ($MPTB_P$) were isolated. In the latter system two other phases were also synthesized: $Na_4Nb_8P_6O_{35}$[20] related to the hypothetical $m = 3$ member of the series of diphosphate tungsten bronzes with pentagonal tunnels ($DPTB_P$) and $Na_6Nb_8P_5O_{35}$,[21] whose structure exhibits a great similarity with the niobium disilicate $Ba_3Nb_6Si_4O_{26}$.

We report here on the magnetic and electron-transport properties of these phases, and we discuss their relation with the crystal structure.

Experimental Section

Polycrystalline samples were prepared according to the standard solid-state reactions previously described for these compounds.[12-20]

Attempts to grow single crystals were made for all the phases. Single crystals of good size could be obtained up to now for only $KNb_3P_3O_{15}$ and β-$K_2Na_2Nb_8P_5O_{34}$ (Figure 1). They were obtained by melting mixtures of niobium phosphate and alkaline chloride, in the molar ratio 4:1 at 1473 K and cooling at a rate of 1 °C h^{-1} to room temperature.

For all other samples bar shaped pellets were made for the electrical measurements. The powder of niobium phosphate was pressed into a bar, sealed in an evacuated quartz tube, and "sintered" at the reaction temperature for 4 days.

Electrical measurements were performed by a four-probe standard technique from 4.5 K to room temperature.

(1) Raveau, B. *Proc. Indian Acad. Sci. (Chem. Sci.)* **1986**, *96*, 419.
(2) Raveau, B. *Proc. Indian Acad. Sci. Acad.* **1986**, *A52*, 67.
(3) Wang, E.; Greenblatt, M.; Rachedi, I.E.-I.; Canadell, E.; Whangbo, M.-H. *Inorg. Chem.* **1989**, *28*, 2451.
(4) Canadell, E.; Rachedi, I.E.-I.; Wang, E.; Greenblatt, M.; Whangbo, M.-H. *Inorg. Chem.* **1989**, *28*, 2455.
(5) Wang, E.; Greenblatt, M.; Rachedi, I.E.-I.; Canadell, E.; Whangbo, M.-H.; Vadlamannati, S. *Phys. Rev.* **1989**, *B39*, 12969.
(6) Wang, E.; Greenblatt, M.; Rachedi, I.E.-I.; Canadell, E.; Whangbo, M.-H. *J. Solid State Chem.* **1989**, *80*, 266.
(7) Wang, E.; Greenblatt, M.; Rachedi, I.E.-I.; Canadell, E.; Whangbo, M.-H. *J. Solid State Chem.* **1989**, *81*, 173.
(8) Teweldemedhin, Z. S.; Ramanujachary, K. V.; Greenblatt, M. *J. Solid State Chem.* **1991**, *95*, 21.
(9) Teweldemedhin, Z. S.; Ramanujachary, K. V.; Greenblatt, M. *Phys. Rev.* **1992**, *B46*, 7897.
(10) Canadell, E.; Whangbo, M.-H.; Rachedi, I.E.-I. *Inorg. Chem.* **1990**, *29*, 3871.
(11) Canadell, E.; Whangbo, M.-H. *Phys. Rev.* **1991**, *B39*, 1894.
(12) Leclaire, A.; Borel, M. M.; Grandin, A.; Raveau, B. *J. Solid State Chem.* **1989**, *80*, 12.
(13) Benabbas, A.; Borel, M. M.; Grandin, A.; Leclaire, A.; Raveau, B. *J. Solid State Chem.* **1990**, *84*, 365.
(14) Leclaire, A.; Benabbas, A.; Borel, M. M.; Grandin, A.; Raveau, B. *J. Solid State Chem.* **1989**, *83*, 245.
(15) Benabbas, A.; Borel, M. M.; Grandin, A.; Leclaire, A.; Raveau, B. *J. Solid State Chem.* **1990**, *87*, 360.
(16) Benabbas, A.; Borel, M. M.; Grandin, A.; Chardon, J.; Leclaire, A.; Raveau, B. *J. Solid State Chem.* **1991**, *91*, 323.
(17) Costentin, G.; Borel, M. M.; Grandin, A.; Leclaire, A.; Raveau, B. *Mater. Res. Bull.* **1991**, *26*, 1051.
(18) Benabbas, A.; Leligny, H.; Borel, M. M.; Grandin, A.; Leclaire, A.; Raveau, B. *J. Solid State Chem.* **1992**, *101*, 137.
(19) Benabbas, A.; Borel, M. M.; Grandin, A.; Leclaire, A.; Raveau, B. *J. Solid State Chem.* **1991**, *95*, 245.
(20) Benabbas, A.; Borel, M. M.; Grandin, A.; Leclaire, A.; Raveau, B. *J. Solid State Chem.* **1990**, *89*, 75.
(21) Benabbas, A.; Borel, M. M.; Grandin, A.; Leclaire, A.; Raveau, B. *J. Solid State Chem.* **1991**, *92*, 51.

0897-4756/93/2805-1143$04.00/0

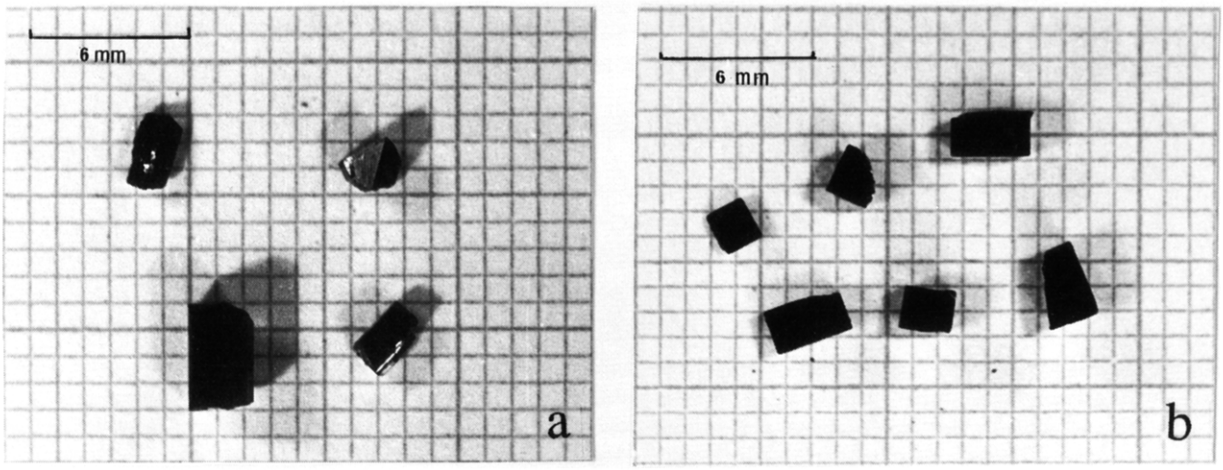

Figure 1. Single crystals of (a) $KNb_3P_3O_{15}$ and (b) β-$K_2Na_{2-x}Nb_8P_5O_{35}$.

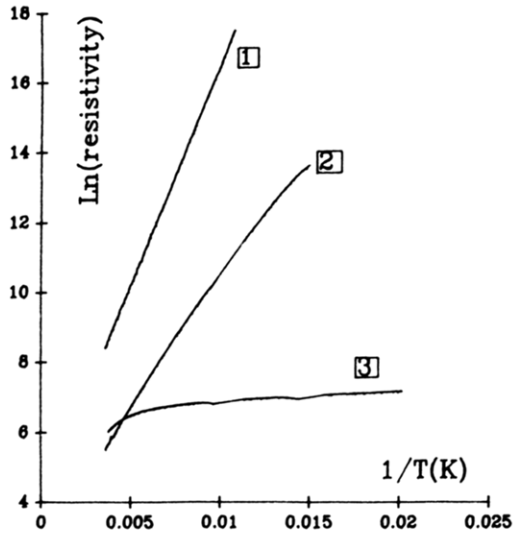

Figure 2. Logarithmic plot of the electrical resistivity vs $1/T$ for (1) $K_3Na_3Nb_8P_5O_{35}$, (2) $Na_4Nb_7P_4O_{29}$, and (3) $K_2Na_2Nb_8P_6O_{35}$.

The magnetic susceptibility was recorded with a Quantum Design SQUID magnetometer in the temperature range 4.5–300 K.

Results and Discussion

Sodium Phosphate Bronzes. The difficult synthesis of the phases of the system Na–Nb–P–O has not allowed, up to now, sufficiently large single crystals to be grown. Moreover, for many of those phases, the quality of the sintered bars was poor, so that electrical measurements were not significant. In some cases, partial substitution of potassium was necessary to stabilize the phase during sintering. For these reasons, the investigation of electron transport properties could be performed on only three phases: $K_3Na_3Nb_8P_5O_{35}$, $K_2Na_2Nb_8P_6O_{35}$, and $Na_4Nb_7P_4O_{29}$.

The temperature dependence of the electrical resistivity of these phases is shown in Figure 2. All samples exhibit a semiconductor behavior. However, one observes that the phosphate $K_3Na_3Nb_8P_5O_{35}$ is much more resistive than the two other phases, $Na_4Nb_7P_4O_{29}$ and $K_2Na_2Nb_8P_6O_{35}$. But the most important difference deals with the low activation energy of the phosphate $K_2Na_2Nb_8P_6O_{35}$ of 0.001 eV, compared to $Na_4Nb_7P_4O_{29}$ (0.064 eV) and to $K_3Na_3Nb_8P_5O_{35}$ (0.109 eV). Thus the behavior of $K_2Na_2Nb_8P_6O_{35}$ appears to be very close to that of a semimetal, whereas the semiconducting character increases for $Na_4Nb_7P_4O_{29}$ and especially for $K_3Na_3Nb_8P_5O_{35}$.

The disappointing properties of these niobium bronzes compared to the metallic or semimetallic characteristics of the tungsten phosphate bronzes can be understood by considering their structure and also the electron carrier density.

The semiconducting behavior of the phosphate $K_3Na_3Nb_8P_5O_{35}$ is explained by the absence, in its structure (Figure 3), of octahedral chains belonging to the ReO_3-type, i.e., with Nb–O–Nb angles of 180° or 90° that would allow an efficient overlapping of the niobium d-orbitals with oxygen p-orbitals. The $[Nb_8P_6O_{35}]_\infty$ framework forms $[Nb_8P_2O_{29}]_\infty$ conducting layers separated by insulating $[P_3O_6]_\infty$ layers (Figure 3a). Though in the $[Nb_8P_2O_{29}]_\infty$ layers (Figure 3b) the NbO_6 octahedra share their corners, leading to a bidimensional conductivity, they form Nb–O–Nb angles far from 180°, that hinder an efficient overlapping of d-Nb orbitals and p-O orbitals. Such a situation is also observed in the hexagonal tungsten bronzes A_xWO_3(HTB), with a rather similar tilting of the WO_6 octahedral in the (001) plane. However, in the HTBs, a good overlapping of the orbitals is ensured by the octahedral ReO_3-type chains running along $\vec{c}$, that allows a complete delocalization of the electrons leading to metallic properties. Moreover, the charge balance of this phase, according to the formulation $Na_3K_3Nb^V_7Nb^{IV}P_5O_{35}$ shows that the electron carrier density is low, less than 0.12 e/niobium compared to $K_{0.33}WO_3$ (0.33 e/tungsten). The tendency of localization of electrons in this phosphate is also supported by the bond valence calculations applied to $Na_6Nb_8P_5O_{35}$.[20] The latter show indeed that the Nb(1) octahedra forming the Nb_6O_{27} units of the $[Nb_8P_2O_{29}]_\infty$ layers (Figure 3b) contain extra electrons (Nb^V–Nb^{IV}), whereas the Nb(2) octahedra which ensure the connection between the Nb_6O_{27} units do not have extra electrons (Nb^V). The temperature dependence of the inverse magnetic susceptibility of $Na_3K_3Nb_8P_5O_{35}$ (Figure 4) follows the Curie–Weiss law with a Curie constant C = 0.356, an effective magnetic moment, μ_{eff} = 1.69 μ_B close to the theoretical value (1.73 μ_B), and an extrapolated Curie temperature, θ = −33 K.

The semiconducting properties of the phosphate $Na_4Nb_7P_4O_{29}$ are at first sight surprising if one considers the metallic properties of the monophosphate bronze $P_4W_8O_{32}$[9] which belongs to the same structural family ($MPTB_p$). The structure of this niobium phosphate (Figure 5a) is indeed built up from ReO_3-type layers, which are four and

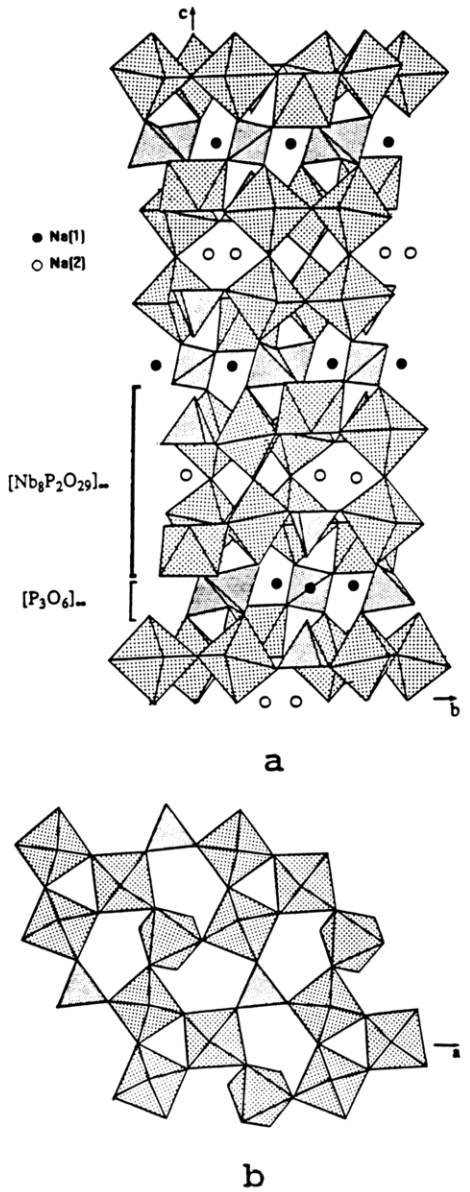

Figure 3. Structure of $K_3Na_3Nb_8P_5O_{35}$: (a) projection along $\vec{a}$; (b) $[Nb_8P_2O_{29}]_\infty$ layers.

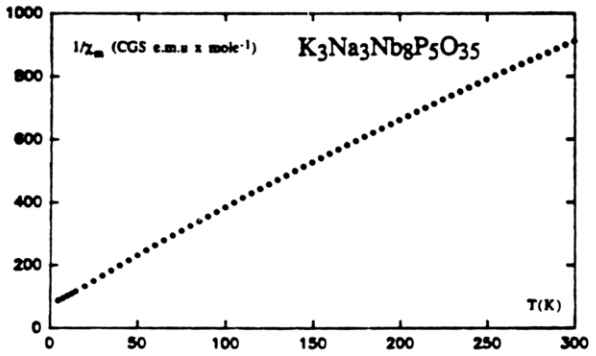

Figure 4. Inverse magnetic susceptibility vs temperature for $K_3Na_3Nb_8P_5O_{35}$.

three NbO_6 octahedra wide alternately, connected through insulating layers of PO_4 tetrahedra. Two factors can explain this difference:

(*i*) *The low electron carrier density of* $Na_4Nb_7P_4O_{29}$: The charge balance of this phase, deduced from its formula $Na_4Nb^V_6Nb^{IV}P_4O_{29}$, shows that the maximum electron density of 0.14 e/niobium is small compared to that expected for $P_4W^V_4W^{VI}_4O_{32}$, of 0.5 e/tungsten.

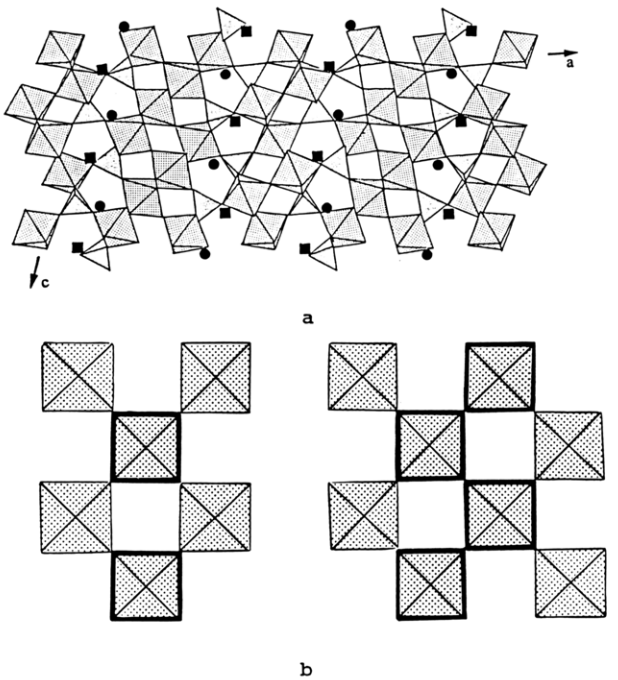

Figure 5. Structure of $Na_4Nb_7P_4O_{29}$: (a) projection along $\vec{b}$; (b) blocks $m = 3$ and $m = 4$.

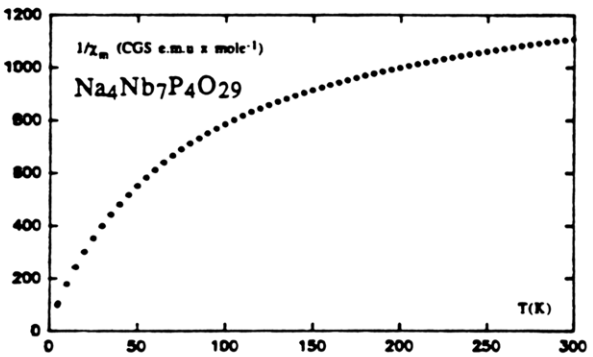

Figure 6. Inverse magnetic susceptibility vs temperature for $Na_4Nb_7P_4O_{29}$.

(*ii*) *A larger distortion of the* NbO_6 *octahedra and especially a tilting of these octahedra* leading to a significant deviation of the Nb–O–Nb angles from 180° and 90°: This phenomenon observed in the pure isotypic Nb^V phosphate $Na_3Nb_7P_4O_{29}$[17] cannot be transposed directly to the mixed-valent phase $Na_4Nb_7P_4O_{29}$. Nevertheless, there is no doubt that the phosphate groups are accommodated more easily by the WO_6 octahedra than by the NbO_6 octahedra. This phenomenon results in a significant deformation of the octahedral framework which may affect the overlapping of the niobium d-orbitals with oxygen p-orbitals in $Na_4Nb_7P_4O_{29}$.

It appears likely that the extra electron of $Na_4Nb_7P_4O_{29}$ should be mainly distributed on the NbO_6 octahedra located inside the ReO_3-type layers, whereas the NbO_6 octahedra located on the border of the layers, i.e., linked to the PO_4 tetrahedra, would be mainly occupied by Nb^V, which allows a larger distortion of these octahedra (Figure 5b). According to this hypothesis, one row of octahedra out of three would contain the extra electron in the $m = 3$ layer, whereas two rows out of four can accept this electron in the $m = 4$ layer as schematized on Figure 5b. This model is strongly supported by the curve $1/\chi = f(T)$ (Figure 6) which can be fitted by considering the two different ReO_3-type slabs, $m = 3$ and $m = 4$. If one neglects

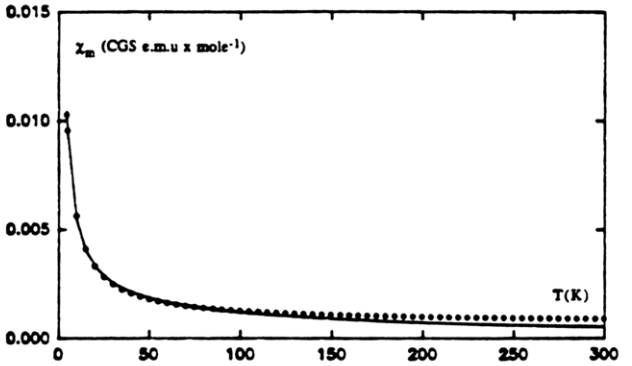

Figure 7. Magnetic susceptibility $\chi_m = f(T)$ for $K_2Na_2Nb_8P_6O_{35}$ (···) experimental curve and (—) fitted curve: $\chi = (C/T) + (C'/T - \theta)$.

the magnetic interactions between two successive slabs since they are separated by PO_4 groups, the magnetic susceptibility can be considered as the sum of the contributions of the two different slabs, $m = 3$ and $m = 4$. Moreover, in the $m = 3$ slabs, the magnetic interations can be considered as negligible since only the intermediate octahedral row contains extra electrons (Figure 5b), so that each of the corresponding NbO_6 octahedra is isolated. Thus the magnetic susceptibility can be written in the following way:

$$\chi = \chi_{m=3} + \chi_{m=4} = \frac{C}{T} + \frac{C'}{T - \theta} \qquad (1)$$

Owing to the low values of the magnetic susceptibility above 100 K, the fitting of this experimental curve (Figure 7) according to eq 1 could only be made below this temperature. The values obtained for the constants are $C = 0.040$, $C' = 0.155$, and $\theta = -95.5$ K. The two effective moments which can be deduced are of 0.57 and 1.11 μ_B which would correspond to the $m = 3$ and $m = 4$ ReO_3-type slabs, respectively. The latter values imply a distribution of the extra electronic charge for 34% in the $m = 3$ layer and 66% in the $m = 4$ layer, in agreement with our above hypothesis which suggests that one row of NbO_6 octahedra contains the extra charges in the $m = 3$ slabs against two in the $m = 4$ slabs.

The higher conductivity of $K_2Na_2Nb_8P_6O_{35}$ and especially its small activation energy are easily explained by the significantly higher electron carrier density, which can reach 0.5 electron/niobium like in the tungsten phosphate bronzes. The structure of this phase (Figure 8) isotypic with $Na_4Nb_8P_6O_{35}$[19] shows that the NbO_6 octahedra are connected in a bidimensionnal way. One observes $[NbO_3]_\infty$ zig-zag chains running along $\vec{a}$ (Figure 8a) that exhibit close relationships with the perovskite structure and $[Nb_4O_{11}]_\infty$ chains running along $\vec{c}$ (Figure 8b), involving "Nb_2O_{10}" units of two edge-sharing octahedra. Nevertheless, according to the results obtained for $Na_4Nb_8P_6O_{35}$, the octahedra remain significantly distorted and the Nb–O–Nb angles in the chains are significantly different from 180° and 90°, so that the overlapping is still insufficient to allow a metallic conductivity. Moreover the valence bond calculations show a preferential localisation of the electron in the Nb_2O_{10} units,[19] which are occupied by Nb^{IV} to decrease the coulombic repulsion, whereas the other octahedra are characterized by a mixed valence of niobium, Nb^{IV}–Nb^{V}. The inverse magnetic susceptibility curve of this phase (Figure 9) shows also a particular behaviour due to the presence of three different sites Nb(1), Nb(2), and Nb(3). For its interpretation, the exchange magnetic

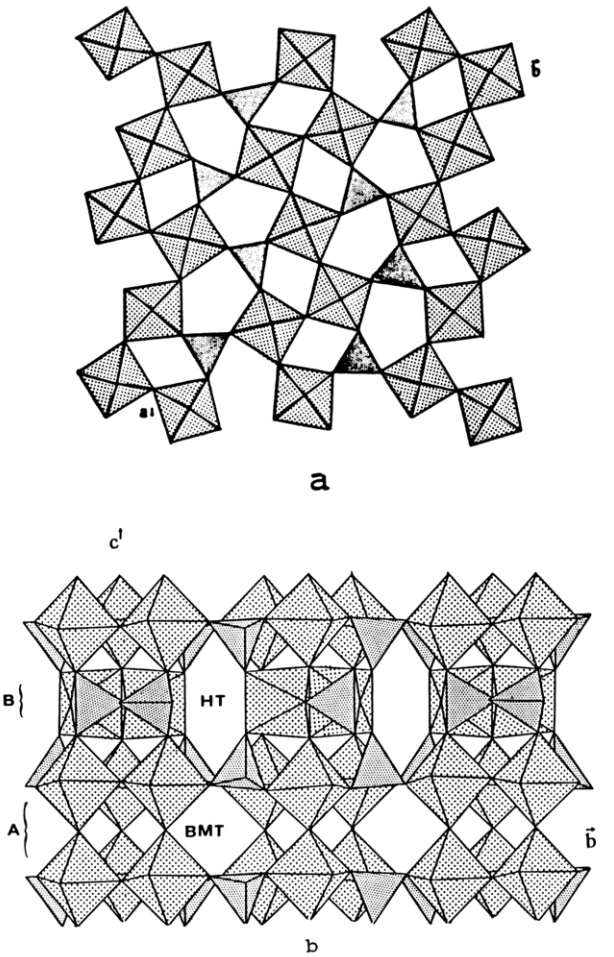

Figure 8. Structure of $K_2Na_2Nb_8P_6O_{35}$: (a) $[Nb_3P_2O_{17}]$ layers; (b) projection along $\vec{a}$.

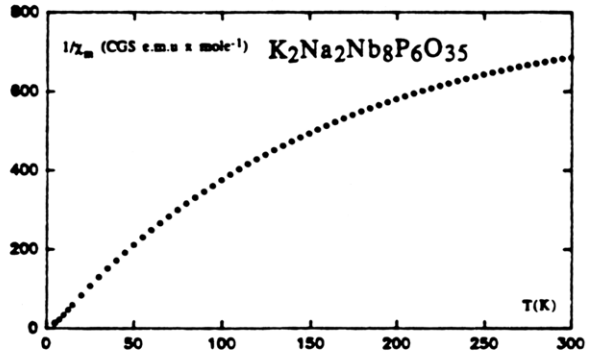

Figure 9. Inverse magnetic susceptibility vs temperature for $K_2Na_2Nb_8P_6O_{35}$.

fields can be written as a function of the magnetic moments in the following way:

$$B_1 = \alpha M_1 + \beta M_3$$

$$B_2 = M_2 + 2\omega M_3$$

$$B_3 = 2\beta M_1 + 2\omega M_2 + \lambda M_3$$

with

$$\frac{M_1}{B_a + B_1} = \frac{C_1}{T}; \quad \frac{M_2}{B_a + B_2} = \frac{C_2}{T}; \quad \frac{M_3}{B_a + B_3} = \frac{C_3}{T}$$

where B_a is the applied magnetic field.

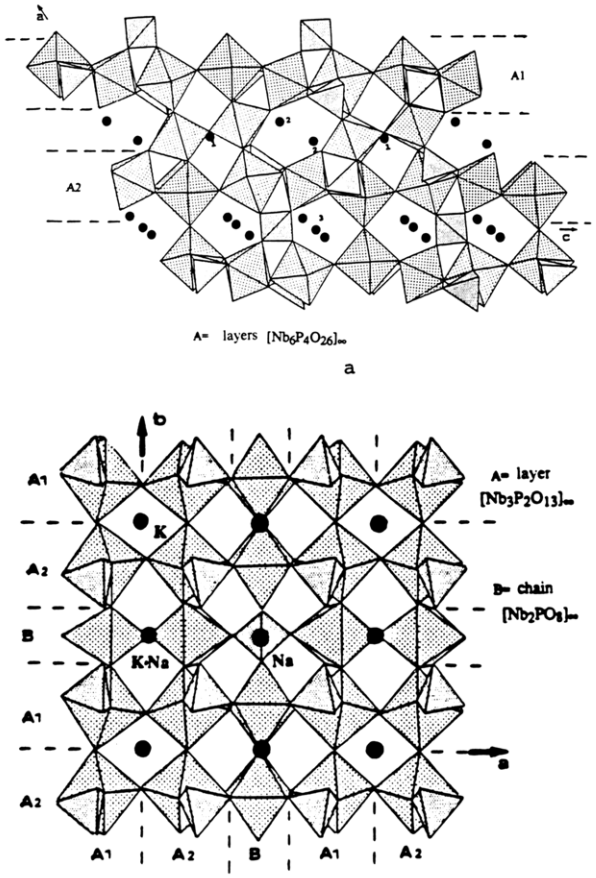

Figure 10. Projections of the structure of (a) α-$K_{5-x}Nb_8P_5O_{34}$ along $\vec{b}$ and (b) β-$K_2Na_{2-x}Nb_8P_5O_{34}$ along $\vec{c}$.

Then the magnetic susceptibility deduced from these equations is

$$\chi = \frac{M_1 + M_2 + M_3}{B_a} + \frac{AT^2 + BT^2 + C}{T^3 + DT^2 + ET + F} \qquad (2)$$

Potassium Phosphate Bronzes. The physical measurements were performed on five compounds: $K_7Nb_{14}P_9O_{60}$,[14] $K_3Nb_6P_4O_{26}$,[13] α-$K_5Nb_8P_5O_{34}$,[15] β-$K_2Na_2Nb_8P_5O_{34}$,[16] and $KNb_3P_3O_{15}$.[12] A general features of all these compounds deals with their electrical resistivity much higher than those observed for the sodium phosphates.

The two phases α-$K_5Nb_8P_5O_{34}$ and β-$K_2Na_2Nb_8P_5O_{34}$ are practically insulators, with a resistivity larger than 10^7 Ω cm at room temperature for a single crystal of the second phase. In both structures one observes $[NbO_3]_\infty$ chains of corner-sharing octahedra forming mixed layers of corner-sharing NbO_6 octahedra and PO_4 tetrahedra in which the NbO_6 octahedra are interconnected making possible the displacement of electrons along the chains (Figure 10). However in these structures the geometry of the $[NbO_3]_\infty$ chains is very different from that of the ReO_3-type chains as shown for instance from Figure 11 where it can be seen that the Nb–O–Nb angles are much closer to 60–120° than to 180–90°. This may explain the very high resistivity of these phases, compared to the sodium phosphates, in spite of the similar potential electrons carrier density of 0.25 e/niobium for α-$K_5Nb^V_6Nb^{IV}_2P_5O_{34}$ and of 0.12 e/niobium for β-$K_2Na_2Nb^V_7Nb^{IV}P_5O_{34}$.

The temperature dependence resistivity of the three phosphates $K_7Nb_{14}P_9O_{60}$, $K_3Nb_6P_4O_{26}$, and $KNb_3P_3O_{15}$ (Figure 12), shows that they exhibit like sodium phosphates

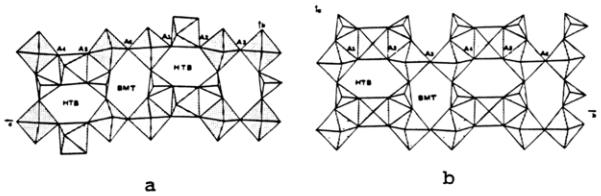

Figure 11. $[Nb_3P_2O_{13}]_\infty$ layers: (a) in α-$K_{5-x}Nb_8P_5O_{34}$ and (b) in β-$K_2Na_{2-x}Nb_8P_5O_{34}$.

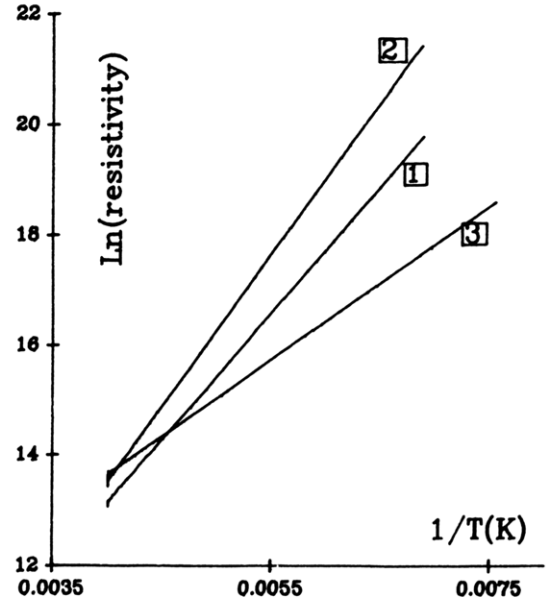

Figure 12. Temperature of the ln ρ for (1) $K_3Nb_6P_4O_{26}$, (2) $K_7Nb_{14}P_9O_{60}$, and (3) $KNb_3P_3O_{15}$.

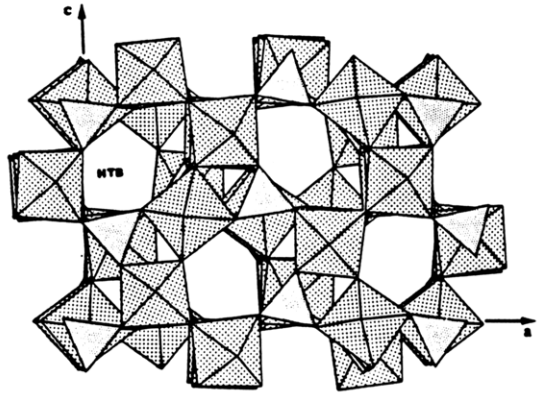

Figure 13. Projection of the structure of $K_3Nb_6P_4O_{26}$ along $\vec{c}$.

a semiconducting behavior. Nevertheless their conductivity at room temperature ranging from 8×10^3 Ω cm for $KNb_3P_3O_{15}$ to (5–7) $\times$ 10^4 Ω cm for $K_7Nb_{14}P_9O_{60}$ and $K_3Nb_3P_4O_{26}$ is 1–2 orders of magnitude larger than those observed for the sodium phosphates in spite of their potential electron carrier density; indeed, according to their formula $K_7Nb^V_{12}Nb^{IV}_2P_9O_{60}$, $K_3Nb^V_5Nb^{IV}_1P_4O_{26}$, and $KNb^V_2Nb^{IV}_1P_3O_{15}$, these phosphates may reach up to 0.04, 0.16 and 0.33 electron/niobium, respectively. In the same way the activation energies of 0.239 and 0.199 eV for $K_7Nb_{14}P_9O_{60}$ and $K_3Nb_6P_4O_{26}$ are significantly higher than those of the sodium phase, whereas the activation energy of $KNb_3P_3O_{15}$ of 0.12 eV is still superior to that of $K_3Na_3Nb_8P_5O_{35}$. This semiconducting character is easily understood by considering the structure of these bronzes. Indeed in both structures $K_3Nb_6P_4O_{26}$ (Figure 13) and $K_7Nb_{14}P_9O_{60}$ (Figure 14), one observes $[NbO_3]_\infty$ chains of corner-sharing octahedra which are three-dimensionally

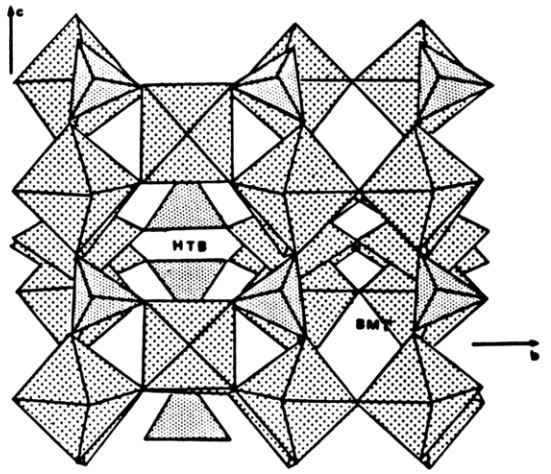

Figure 14. Projection of the structure of $K_7Nb_{14}P_9O_{60}$ along $\vec{a}$.

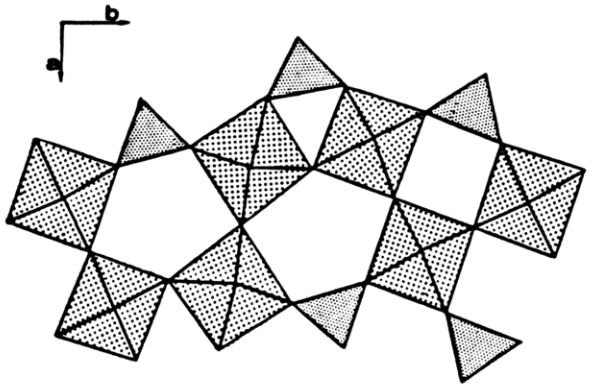

Figure 15. $[NbO_3]_\infty$ chain parallel to $\vec{b}$ in $KNb_3P_3O_{15}$.

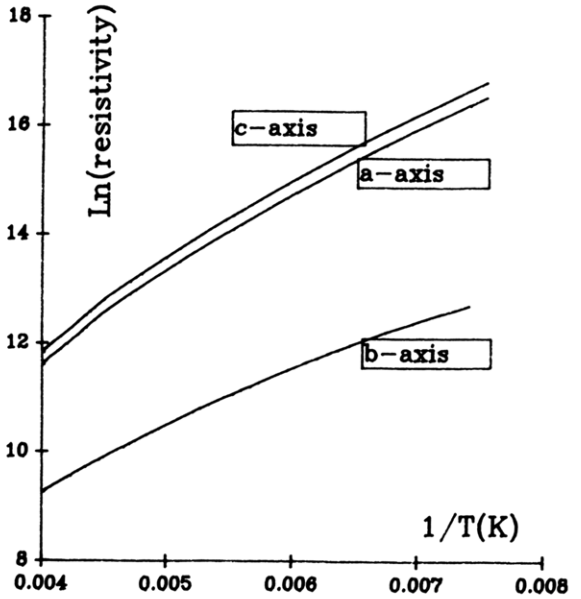

Figure 16. Figure shows ln ρ vs $1/T$ of $KNb_3P_3O_{15}$ single crystal along the three directions $\vec{a}$, $\vec{b}$, and $\vec{c}$.

interconnected; but unfortunately, the geometry of these chains is not favorable to the overlapping of the orbitals of niobium and oxygen since they form Nb–O–Nb angles intermediate between 120° and 180°, and moreover the NbO_6 octahedra are significantly distorted. In the $KNb_3P_3O_{15}$ structure (Figure 15), the NbO_6 octahedra form $[NbO_3]_\infty$ ribbons with the TTB structure running along $\vec{b}$; these ribbons are isolated from each other, i.e., are linked only through PO_4 tetrahedra so that they should only be considered as unidimensional conductors. Again in these

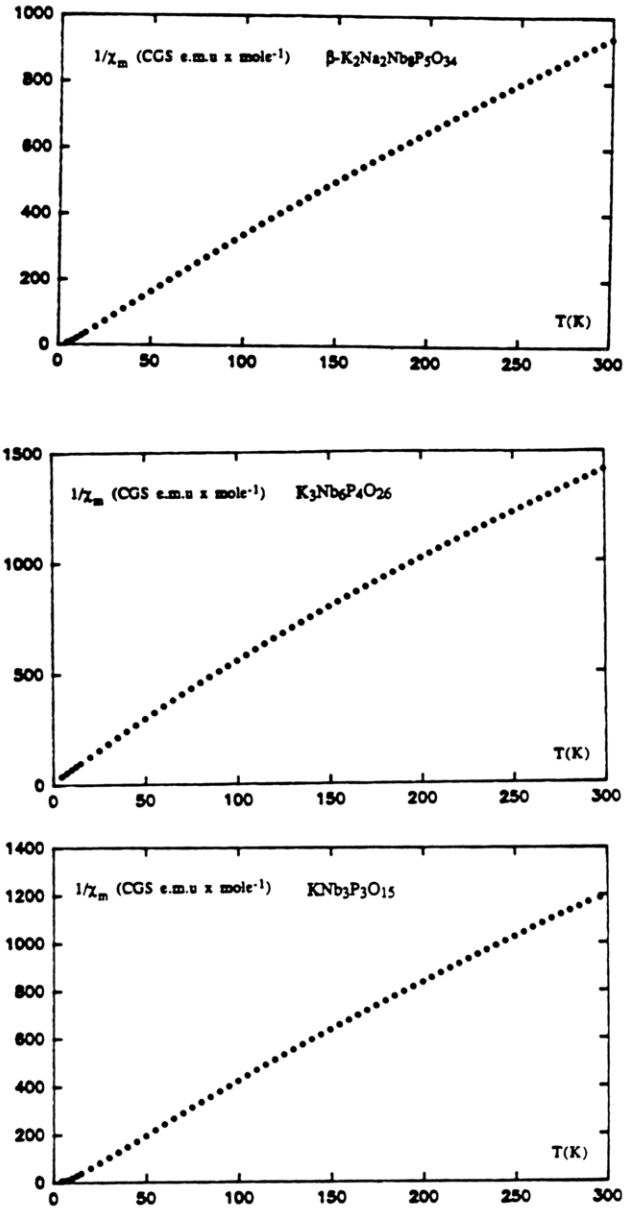

Figure 17. Inverse magnetic susceptibility vs temperature for β-$K_2Na_{2-x}Nb_8P_5O_{34}$, $K_3Nb_6P_4O_{26}$, and $KNb_3P_3O_{15}$.

chains it can be seen that besides O–Nb–O angles of 180°, there exist Nb–O–Nb angles intermediate between 120° and 180° so that the overlapping of the Nb and O orbitals are not optimal, explaining their semiconducting properties. Nevertheless, resistivity measurements performed on single crystals of this latter phase have allowed to show its anisotropic character. One indeed observes from the curves ln $\rho = f(T)$ (Figure 16) that the resistivity along $\vec{b}$ is nearly 1 order of magnitude lower than along the two other directions (1.1×10^3 Ω cm against ($1.3–1.6$) $\times 10^4$ Ω cm at room temperature); in the same way the activation energy of this phase along $\vec{b}$, of 0.089 eV, is smaller than along $\vec{a}$ (0.124 eV) and along $\vec{c}$ (0.126 eV). These observations confirm the unidimensional character of the conductivity, in agreement with the direct connection of the NbO_6 octahedra along $\vec{b}$, whereas in the two other directions the junction between these octahedra is ensured by PO_4 tetrahedra.

The reciprocal susceptibility of the three compounds, β-$K_2Na_2Nb_8P_5O_{34}$, $K_3Nb_6P_4O_{26}$, and $KNb_3P_3O_{15}$ versus temperature (Figure 17) follows the Curie law, whereas for the phases $K_7Nb_{14}P_9O_{60}$ and α-$K_5Nb_8P_5O_{34}$ one

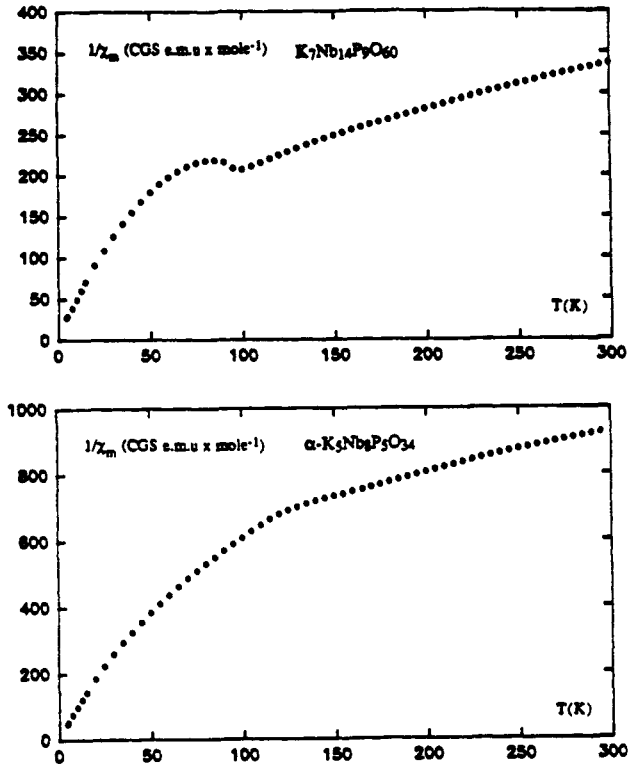

Figure 18. Inverse magnetic susceptibility vs temperature for α-$K_{5-x}Nb_8P_5O_{34}$ and $K_7Nb_{14}P_9O_{60}$.

observes a Curie–Weiss behavior only at high temperature (Figure 18). The anomalies apparent in Figure 18 may be due to magnetic interactions rather than structural phase transitions. The Curie constants and the deduced effective moments of these phases are reported in Table I. The values of μ_{eff} observed of 1.64 and 1.74 μ_B observed for β-$K_2Na_2Nb_8P_5O_{34}$ and $K_7Nb_{14}P_9O_{60}$, respectively, are in agreement with the theoretical value of Nb^{IV} (1.55 or 1.73 μ_B). The slightly smaller values of μ_{eff}, ranging from 1.28 to 1.434 μ_B observed for the three other phases, $K_3Nb_6P_4O_{26}$, $KNb_3P_3O_{15}$, and α-$K_5Nb_8P_5O_{34}$ is easily explained by a small potassium deficiency, leading to a higher

Table I. Magnetic Susceptibility

compounds	C	μ_{eff} (μ_B)
β-$K_2Na_2Nb_8P_5O_{34}$	0.340	1.649
$K_3Nb_6P_4O_{26}$	0.232	1.636
$KNb_3P_3O_{15}$	0.257	1.434
$K_7Nb_{14}P_9O_{60}$	1.516	1.74
α-$K_5Nb_8P_5O_{34}$	0.820	1.28

Nb^V content; this deviation from stoichiometry has indeed been confirmed for $K_{4-x}Nb_6P_4O_{26}$ with x ranging from 0 to 2.[22] The phosphates $K_7Nb_{14}P_9O_{26}$ and α-$K_5Nb_8P_5O_{34}$ exhibit an unusual behavior at low temperature. One observes (Figure 18) a sharp decrease of χ_m^{-1} for $K_7Nb_{14}P_9O_{60}$, and a broader one for α-$K_5Nb_8P_5O_{34}$ as the temperature decreases. This anomaly which starts around 100 K, can be attributed to a phase transition. A resolution of these structures at low temperatures will be necessary to confirm this hypothesis.

Concluding Remarks

The investigation of the electron-transport properties of the niobium phosphate bronzes shows that these materials are all semiconductors, contrary to the phosphate tungsten bronzes which are metallic, in spite of the analogous properties of the mixed valencies Nb^{IV}–Nb^V and W^V–W^{VI}. This absence of metallic properties can be easily understood for most of the structures, on the basis of the geometry of the $[NbO_3]_\infty$ chains. The latter exhibit distorted NbO_6 octahedra but also are characterized by Nb–O–Nb angles different from 180–90°, so that the overlapping of the d-orbitals of niobium and p-orbitals of oxygen is hindered. Moreover the potential electron carrier density deduced from the chemical formula, in these oxides, is generally rather low compared to the tungsten phosphate bronzes. Attempts to synthesize new materials in this series with higher Nb^{IV} contents, and varying the geometry of the $[NbO_3]_\infty$ chains should allow metallic properties to be obtained.

(22) Borel, M. M.; Grandin, A.; Benabbas, A.; Leclaire, A.; Raveau, B. *Mater. Res. Bull.* **1989**, *24*, 1485.